24th INTERNATIONAL CONGRESS ON SOUND AND VIBRATION
23–27 July 2017, London

ICSV24
23-27JULY 2017
LONDON CALLING

AIRFOIL LEADING EDGE NOISE PREDICTIONS USING A VISCOUS MEAN FLOW

Yuhao Sun, Ryu Fattah, and Xin Zhang
The Hong Kong University of Science and Technology, Department of Mechanical and Aerospace Engineering, HKSAR, China.
email: ysunau@connect.ust.hk

The airfoil leading edge noise from a NACA 0012 airfoil at zero degrees angle of attack is numerically modelled using the linearised Euler equations with synthesised turbulence that follows a von-Kármán energy spectra. The differences in the far-field noise based on an inviscid, and viscous, mean flow are investigated. A gradient term suppression model is used to avoid the onset of instabilities generated by the strong shear layer in the viscous mean flows. The mean flow solutions are obtained at free-stream velocities from $20\,\mathrm{m/s}$ to $120\,\mathrm{m/s}$, and the airfoil is subjected to turbulence with an integral length scale of 0.05 chord lengths, and a turbulent intensity of 1.7%. The results show that the differences in the far-field sound between a viscous and an inviscid mean flow, are small for free-stream velocities greater than $90\,\mathrm{m/s}$. When the free-stream is at $20\,\mathrm{m/s}$ a viscous mean flow solution predicts a 5dB lower sound pressure levels, at a reduced frequency of 17. At lower free-stream velocities, a thicker boundary layer is formed along the airfoil, which induces a larger displacement thickness, and reduces the radiated sound levels.

1. Introduction

Airfoil leading edge noise is generated when upstream turbulence impinges on the leading edge of an airfoil. Leading edge noise can be a significant broadband noise source for aircraft engines [1], and wind turbines [2, 3]. The leading edge noise generation mechanism has been studied analytically [4, 5], experimentally [6–8], and by high-order computational simulations [9]. Direct numerical studies can be computationally intensive, and a hybrid computation using linearised governing equations with a prescribed mean flow, and synthesized turbulence, is often used to overcome this problem. The synthesized turbulence can be defined by multiple frequency vortical gusts [9, 10], or synthetic eddies [11–13].

Numerical simulations governed by the linearised Euler equations (LEE) can suffer from Kelvin-Helmholtz (K-H) instabilities in the presence of a strongly sheared background mean flow. A viscous mean flow will contain a strong shear layer in the boundary layer region, and this can trigger the K-H instabilities, and cause an over-prediction in the radiated noise [14]. An inviscid mean flow can prescribe the mean pressure and density fields accurately, and provide a mean velocity field with a weak shear layer. Therefore, inviscid mean flows have been used previously to overcome the K-H instability issues. Differences in the far-field noise by viscous and inviscid mean flows have been reported [9, 15]. However, it is unclear whether these differences are caused by physical means, or by numerical instabilities.

The validity of an inviscid mean flow reduces as the thickness of the boundary layer becomes larger. A thicker boundary layer induces a larger displacement thickness that modifies the effective airfoil thickness and leading edge radius. Thicker boundary layers can be found on airfoils at

lower flow speeds (e.g., wind turbines [3]), or on non-stationary airfoils (e.g., pitching [16]). Under these conditions, a viscous mean flow should be prescribed to the linearised Euler equations, and any numerical instabilities should be avoided. In this paper the airfoil leading edge noise generated by upstream turbulence impinging on the leading edge of a static NACA 0012 airfoil at zero degrees angle of attack is compared between LEE simulations performed at free-stream flow velocities of $u_\infty = \{20, 40, 60, 90, 120\}\,\mathrm{m/s}$, and the results obtained by viscous and inviscid mean flows are compared. The remainder of this paper is arranged as follows. In Section 2 the governing equations and the synthetic turbulence method are described. In Section 3 the differences between a viscous and inviscid mean flow, and their effects on the leading edge noise are discussed. Finally, a summary is given in Section 4.

2. Numerical method

In this work the airfoil leading edge noise for a NACA 0012 airfoil at zero degrees angle of attack, and a chord length of $c = 0.15\,\mathrm{m}$ is predicted in two stages. In the first stage, the mean flow fields are obtained using a commercial computational fluid dynamics (CFD) package. The inviscid mean flows are predicted using a slip-wall boundary condition, and the viscous mean flows are obtained using a no-slip boundary condition and the Reynolds-averaged-Navier-Stokes (RANS) equations with the $k-\omega$ SST turbulence model. The airfoil mesh for the viscous calculations are refined near the wall regions to ensure an adequate boundary layer resolution with $y^+ < 1$.

In the second stage, a high-order finite difference computational aeroacoustics (CAA) solver is used. This solver has been previously applied to duct noise radiation problems [17] and to study the leading edge noise of airfoils [9, 12]. The CAA solver utilises fourth-order spatial schemes [18] and a 4-6 stage Range-Kutta temporal scheme [19]. Non-reflective boundary conditions [20] are applied at the outer edges of the computation domain, and a compact filter [21] is used at the end of each time step to remove spurious oscillations. During the simulations, the Courant-Friedrichs-Lewy (CFL) number is set to be smaller than 0.75. The mean flow is interpolated onto a CAA grid to prescribe the mean flow quantities, and the mean flow gradients that are used in the linearised Euler equations. A modified digital filter [12] is used to synthesize a turbulent flow injected 1.6 chord lengths upstream of the airfoil leading edge. The noise radiated by the turbulence-airfoil interaction is fully resolved up to a reduced frequency of $k = fc/u_\infty = 23$, where f is the frequency, c is the airfoil chord length, and u_∞ is the free-stream velocity. The far-field sound pressure level is calculated by an integral solution of Ffowcs Williams and Hawkings (FW-H) equation [22, 23]. An illustration of this method is shown in Figure 1 .

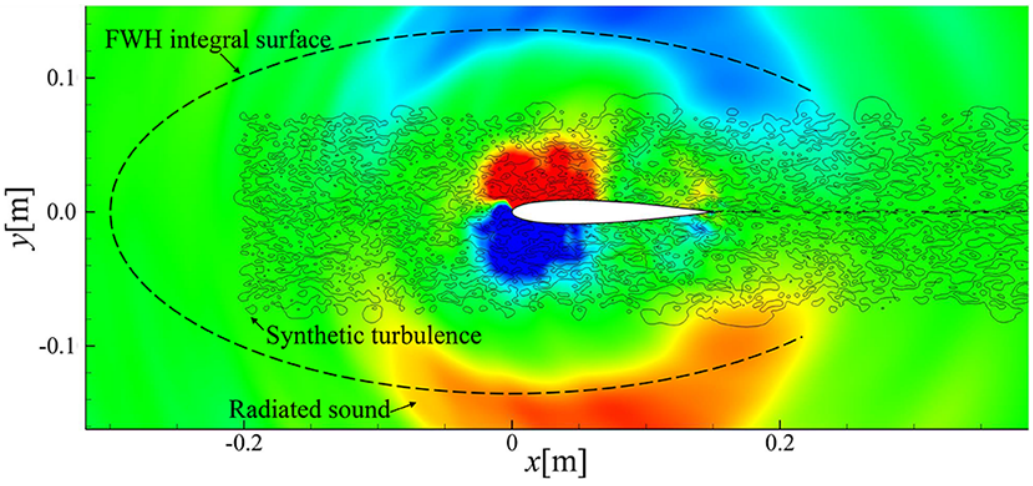

Figure 1: Airfoil leading edge noise simulation schematic.

2.1 Governing equations

The linearised Euler equations are derived by decomposing the flow variables in the Euler equations into its mean and perturbed quantities. By assuming that the perturbed flow quantities are several orders of magnitude smaller than the mean values, the non-linear terms can be neglected, and the Euler equations (in vector notation) becomes:

$$\begin{aligned}
&\frac{\partial \rho'}{\partial t} + \rho' \nabla \cdot \boldsymbol{u}_0 + \rho_0 \nabla \cdot \boldsymbol{u}' + \boldsymbol{u}_0 \cdot \nabla \rho' + \boldsymbol{u}' \cdot \nabla \rho_0 = 0, \\
&\frac{\partial \boldsymbol{u}'}{\partial t} + (\boldsymbol{u}_0 \cdot \nabla)\, \boldsymbol{u}' + (\boldsymbol{u}' \cdot \nabla)\, \boldsymbol{u}_0 + \frac{\nabla p'}{\rho_0} - \frac{\rho'}{\rho_0^2} \nabla p_0 = 0, \\
&\frac{\partial p'}{\partial t} + \boldsymbol{u}_0 \cdot \nabla p' + \boldsymbol{u}' \cdot \nabla p_0 + \gamma \left(p' \nabla \cdot \boldsymbol{u}_0 + p_0 \nabla \cdot \boldsymbol{u}' \right) = 0,
\end{aligned} \tag{1}$$

where t is the time, ρ is the density, p is the pressure, $\boldsymbol{u}$ is the velocity vector, $\gamma = 1.4$ is the ratio of specific heats, and $(\cdot)_0$ and $(\cdot)'$ represent the mean and perturbed quantity, respectively.

The governing equations resolve both acoustic and vortical disturbances. However, the numerical solutions may suffer from K-H instabilities when the mean flow contains a strongly sheared velocity field. By assuming that the mean flow gradients have a negligible effect on the acoustic field, the gradient term suppression (GTS) method [24, 25] can be applied to resolve this numerical issue. The modified momentum equation in GTS is:

$$\frac{\partial \boldsymbol{u}'}{\partial t} + (\boldsymbol{u}_0 \cdot \nabla)\boldsymbol{u}' + \frac{\nabla p'}{\rho_0} - \frac{\rho'}{\rho_0^2} \nabla p_0 = 0. \tag{2}$$

2.2 Synthetic turbulence

The modified digital filter method [12] is used to synthesize quiescent turbulence along an injection region according to a von-Kármán energy spectrum. In the injection region the fluctuating velocity is defined by:

$$\begin{aligned}
u_x(x,y) &= -\epsilon \Delta \sum_{i=1}^{N_e} \frac{\sqrt{2\pi \boldsymbol{u}_{rms,i}^2}}{\Lambda_i^2} (y - y_e) \exp\left(-\frac{\pi r^2}{2\Lambda_i^2} \right), \\
u_y(x,y) &= +\epsilon \Delta \sum_{i=1}^{N_e} \frac{\sqrt{2\pi \boldsymbol{u}_{rms,i}^2}}{\Lambda_i^2} (x - x_e) \exp\left(-\frac{\pi r^2}{2\Lambda_i^2} \right),
\end{aligned} \tag{3}$$

where the subscript N_e is the number of superimposed eddies, u_{rms} is the root-mean-square of the velocity fluctuation, r is the distance taken from the eddy centre (x_e, y_e) to the flow field point (x, y), Δ is the distance between neighbouring eddies, and ϵ randomly takes the value of ± 1. In this work the turbulence was injected 1.6 chord lengths upstream of the airfoil leading edge, and synthesized to have an intensity of $T_u = 1.7\%$ and an integral length of $\Lambda = 0.008$m.

3. Airfoil Leading Edge Noise

3.1 Differences in the airfoil mean flow

Figure 2 shows the pressure profiles measured along the airfoil surface from an inviscid and viscous solver, operating at $u_\infty = 20\,\mathrm{m/s}$ and $u_\infty = 120\,\mathrm{m/s}$. Figure 2 shows that both solvers provide similar pressure and density fields. However, significant differences between the viscous and inviscid velocity profiles are shown in Figure 3. An inviscid solver does not resolve the strong shear layer that is naturally observed in a realistic boundary layer. The remainder of this paper will focus on the effects of the differences in the mean flow, on the leading edge noise characteristics.

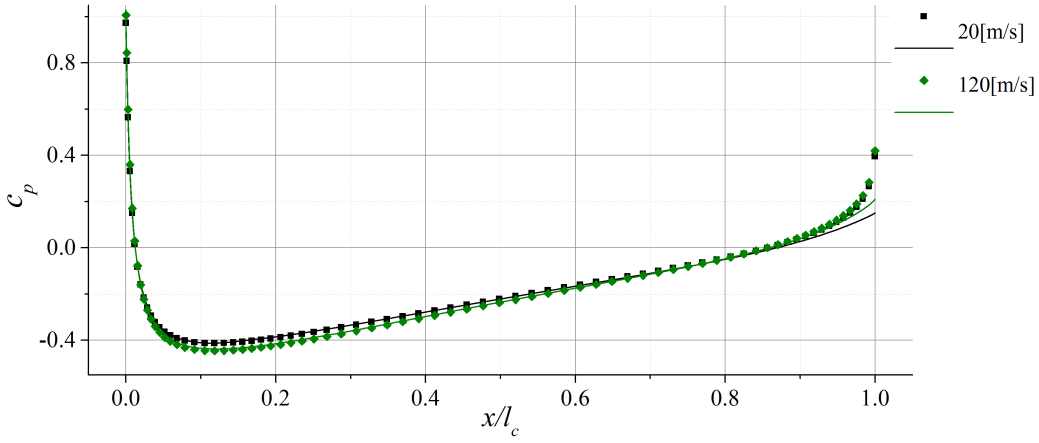

Figure 2: The surface pressure distribution on a NACA 0012 airfoil calculated by an inviscid (symbols) and a viscous (solid line) solver.

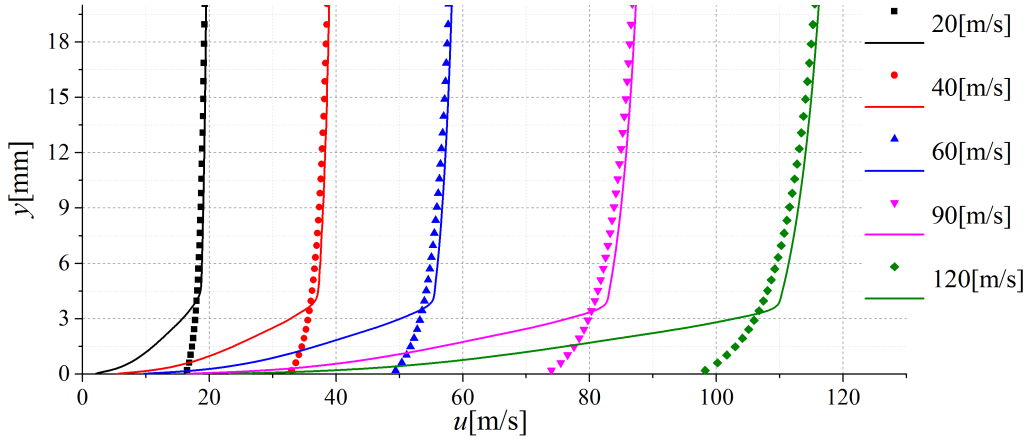

Figure 3: The boundary layer velocity profiles taken at the trailing edge of a NACA 0012 airfoil by an inviscid (symbols) and a viscous (solid line) solver operating at various free-stream velocities.

3.2 Results

The LEE simulations with a viscous mean flow are more prone to K-H instabilities. Figure 4 shows that these instabilities induce spurious strong velocity fluctuations that can interact with the airfoil trailing edge, and cause an over-prediction in the sound power level (PWL) across a wide range of reduced frequencies (Figure 5). By using GTS, the effects of a viscous mean flow can be investigated without the influence of K-H instabilities.

When K-H instabilities are suppressed, the differences in PWL distribution along reduced frequencies between result from a viscous and inviscid mean flow are much less for free-stream velocities of $u_\infty > 90\,\mathrm{m/s}$, as shown in Figure 5.(b) and (c). In this flow regime the assumption of an inviscid mean flow is valid [26]. However, at a free-stream speed of $u_\infty = 60\,\mathrm{m/s}$, a larger deviation is observed at higher reduced frequencies $k > 17$, as shown in Figure 5.(a). This observation is also consistent with [26].

As the free-stream velocity is reduced to $u_\infty < 40\,\mathrm{m/s}$, larger deviations can be observed between results from inviscid mean flows and stabilised viscous mean flows. In Figure 6, the far-field sound pressure field (SPL) directivity plots are given at reduced frequencies of $k = 10$ and $k = 17$, and at free-stream velocities of $u_\infty = 20\,\mathrm{m/s}$ and $u_\infty = 40\,\mathrm{m/s}$. It is shown that over-predicted results are obtained by applying the inviscid mean flow, and the differences are larger at $\theta > 90°$. Additionally, a significant increase in the SPL prediction can be observed if an LEE solution with a realistic mean

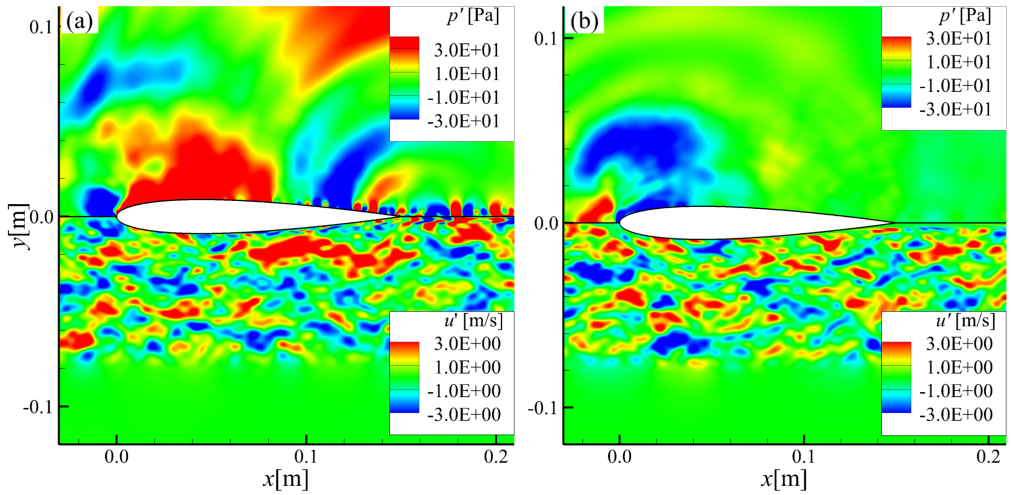

Figure 4: Instantaneous pressure and velocity perturbation contours at $120\,\mathrm{m/s}$ obtained by using (a) LEE and (b) GTS.

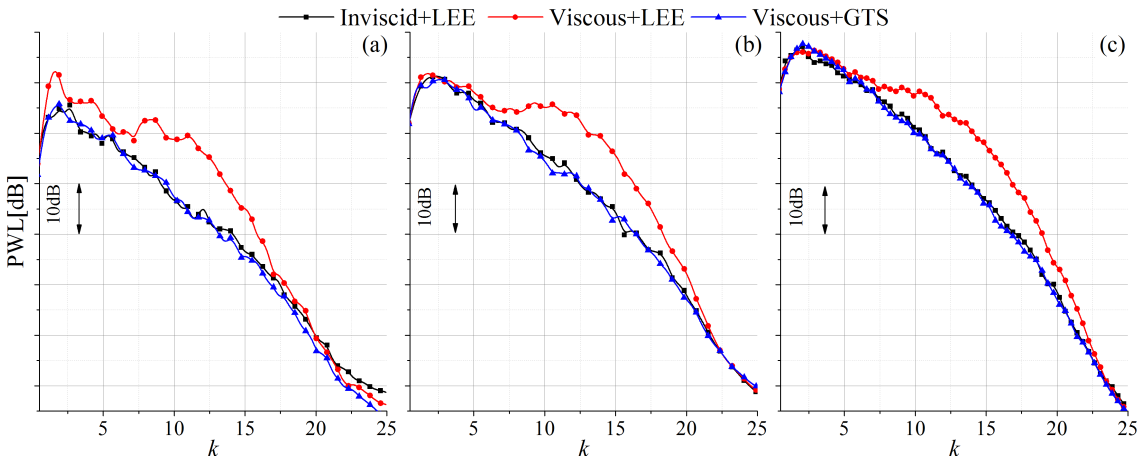

Figure 5: PWL spectra at free-stream velocities of (a) $60\,\mathrm{m/s}$, (b) $90\,\mathrm{m/s}$, and (c) $120\,\mathrm{m/s}$.

flow is attempted without the necessary treatment to remove any K-H numerical instabilities.

The difference of sound energy (ΔE) is determined by measuring the following:

$$\Delta E = \int \left(p'^2_{visc} - p'^2_{inv}\right) \mathrm{d}\theta, \tag{4}$$

where the subscript $(\cdot)_{visc}$ and $(\cdot)_{inv}$ refers to a quantity obtained from a stabilised simulation using a viscous mean flow, and a simulation using an inviscid mean flow, respectively. The velocity scaling of the ΔE is plotted in Figure 7 for three reduced frequencies with the mean flow velocities ranging from $20\,\mathrm{m/s}$ to $120\,\mathrm{m/s}$. It suggests that the boundary layer may have an influence on the dipole noise source, and the effect increases with the decrease of free-stream velocity.

4. Conclusions

In turbulence-airfoil interaction noise studies, the hybrid method using linearised governing equations and synthesized turbulence is often applied for its efficiency, and an inviscid background mean flow is often assumed to avoid the numerical instabilities triggered by the presence of a strongly sheared boundary layer. It is shown that the inviscid mean flow assumption is valid at high free-stream velocities. However, at low free-stream velocities, a viscous mean flow needs to be considered instead since airfoils encounter thicker boundary layers.

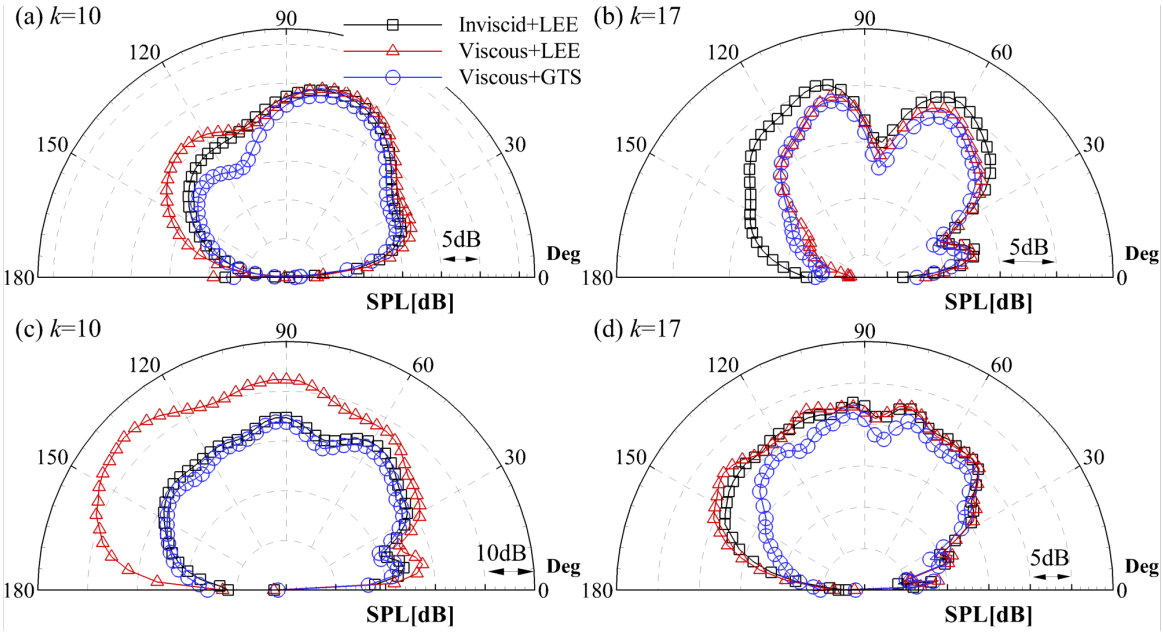

Figure 6: Far-field directivities at $20\,\mathrm{m/s}$ (top) and $40\,\mathrm{m/s}$ (bottom).

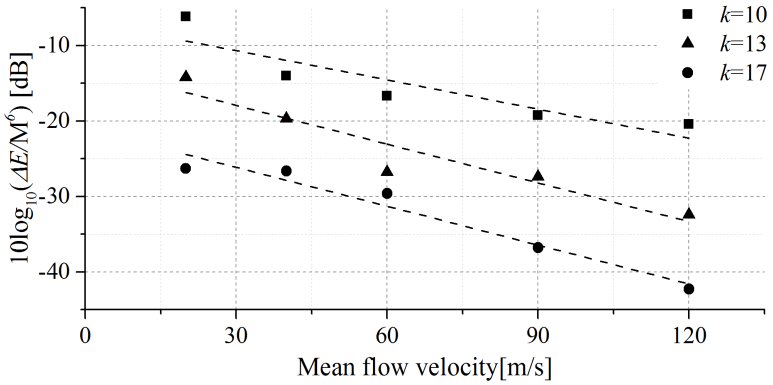

Figure 7: Mach number scaling of ΔE for $k = 10,\ 13,\ \text{and}\ 17$.

High-order CAA leading edge noise simulations were conducted for a NACA 0012 airfoil at zero angle of attack. Far-field noise are calculated with inviscid and viscous mean flows at free-stream velocities ranging from $20\,\mathrm{m/s}$ to $120\,\mathrm{m/s}$. The comparison of inviscid and viscous mean flows shows that viscous mean flows contain stronger shear layers. This strongly sheared boundary layer, coupled with acoustic waves, triggers the numerical K-H instabilities in the CAA simulation, the magnitude of which are to the synthesized turbulence. An additional noise source is generated as the instabilities passing over the trailing edge, and eventually the solution can be contaminated. In this work, the GTS method is applied to overcome this issue with a minor side effect.

After removing the spurious noise source, the effect of using a realistic viscous mean flow was investigated. It is shown that the differences in the noise predictions between viscous and inviscid mean flows are greater at lower free-stream velocities. At $u_\infty = 20\,\mathrm{m/s}$, the simulation with a viscous mean flow predict a noticeable lower far-field sound pressure level at $k > 10$, and the difference is up to $5\,\mathrm{dB}$ at $k = 17$. The over-prediction of the inviscid mean flow calculations scales with the sixth power of the free-stream speed. This suggests that a realistic mean flow is important to the leading edge noise at these high reduced frequencies. A reduced frequency of $k > 10$ may be beyond the area of interest for small bladed problems, but it becomes more significant to engineering applications that focus on larger chord lengths, such as large scale wind turbines.

Acknowledgment

Mr. Yuhao Sun is supported by a PhD fellowship from the Hong Kong University of Science and Technology.

REFERENCES

1. Ganz, U. W., Joppa, P. D., Patten, T. J. and Scharpf, D. F. Boeing 18-inch fan rig broadband noise test, *NASA Contractor Report*, CR-1998-208704, (1998).

2. Glegg, S., Baxter, S. and Glendinning, A. The prediction of broadband noise from wind turbines, *Journal of Sound and Vibration*, **118** (2), 217–239, (1987).

3. Wagner, S., Bareiss, R. and Guidati, G., *Wind turbine noise*, Springer Science & Business Media (2012).

4. Amiet, R. Acoustic radiation from an airfoil in a turbulent stream, *Journal of Sound and Vibration*, **41** (4), 407–420, (1975).

5. Gershfeld, J. Leading edge noise from thick foils in turbulent flows, *The Journal of the Acoustical Society of America*, **116** (3), 1416–1426, (2004).

6. Paterson, R. W. and Amiet, R. Noise and surface pressure response of an airfoil to incident turbulence, *Journal of Aircraft*, **14** (8), 729–736, (1977).

7. Olsen, W. and Wagner, J. Effect of thickness on airfoil surface noise, *AIAA Journal*, **20** (3), 437–439, (1982).

8. Chaitanya, P., Gill, J., Narayanan, S., Joseph, P., Vanderwel, C., Zhang, X. and Ganapathisubramani, B. Aerofoil geometry effects on turbulence interaction noise, *AIAA Paper*, 2015-2830, (2015).

9. Gill, J., Zhang, X. and Joseph, P. Symmetric airfoil geometry effects on leading edge noise, *The Journal of the Acoustical Society of America*, **134** (4), 2669–2680, (2013).

10. Clair, V., Polacsek, C., Le Garrec, T., Reboul, G., Gruber, M. and Joseph, P. Experimental and numerical investigation of turbulence-airfoil noise reduction using wavy edges, *AIAA Journal*, **51** (11), 2695–2713, (2013).

11. Wohlbrandt, A., Guérin, S. and Ewert, R. Simultaneous computation of surface and volume sources for fan broadband noise with the random-particle-mesh method, *AIAA Paper*, 2013-2119, (2013).

12. Gea-Aguilera, F., Zhang, X., Chen, X., Gill, J. R. and Nodé-Langlois, T. Synthetic turbulence methods for leading edge noise predictions, *AIAA Paper*, 2015-2670, (2015).

13. Gea-Aguilera, F., Gill, J., Zhang, X., Chen, X. and Nodé-Langlois, T. Leading edge noise predictions using anisotropic synthetic turbulence, *AIAA Paper*, 2016-2840, (2016).

14. Lockard, D. P. and Morris, P. J. Radiated noise from airfoils in realistic mean flows, *AIAA Journal*, **36** (6), 907–914, (1998).

15. Hainaut, T., Gabard, G. and Clair, V. CAA study of airfoil broadband interaction noise using stochastic turbulent vorticity sources, *AIAA Paper*, 2015-2222, (2015).

16. Bratt, J. Her Majesty's Stationery Office UK, Flow patterns in the wake of an oscillating aerofoil, (1953).

17. Zhang, X. and Chen, X. Broadband wave propagation from an aeroengine duct, *AIAA Journal*, **52** (1), 43–51, (2013).

18. Kim, J. W. Optimised boundary compact finite difference schemes for computational aeroacoustics, *Journal of Computational Physics*, **225** (1), 995–1019, (2007).

19. Hu, F., Hussaini, M. and Manthey, J. Low-dissipation and low-dispersion Runge–Kutta schemes for computational acoustics, *Journal of Computational Physics*, **124** (1), 177–191, (1996).

20. Gill, J., Fattah, R. and Zhang, X. Evaluation and development of non-reflective boundary conditions for aeroacoustic simulations, *AIAA Paper*, 2015-2677, (2015).

21. Kim, J. W. High-order compact filters with variable cut-off wavenumber and stable boundary treatment, *Computers & Fluids*, **39** (7), 1168–1182, (2010).

22. Williams, J. F. and Hawkings, D. L. Sound generation by turbulence and surfaces in arbitrary motion, *Philosophical Transactions of the Royal Society of London A: Mathematical, Physical and Engineering Sciences*, **264** (1151), 321–342, (1969).

23. Brentner, K. S. and Farassat, F. Modeling aerodynamically generated sound of helicopter rotors, *Progress in Aerospace Sciences*, **39** (2), 83–120, (2003).

24. Zhang, X., Chen, X., Morfey, C. and Nelson, P. Computation of spinning modal radiation from an unflanged duct, *AIAA Journal*, **42** (9), 1795–1801, (2004).

25. Bailly, C. and Bogey, C., (2003), Radiation and refraction of sound waves through a two-dimensional shear layer. *Fourth computational aeroacoustics (CAA) workshop on benchmark problems. NASA/CP2004-212954*.

26. Gill, J., Zhang, X. and Joseph, P. Single velocity-component modeling of leading edge turbulence interaction noise, *The Journal of the Acoustical Society of America*, **137** (6), 3209–3220, (2015).